Integration of Solid State Transformer with DC Microgrid System

W. A. Rodrigues, R. A. S. Santana, A. P. L. Cota
Electrical Engineering Graduate Program
Federal University of Minas Gerais (UFMG)
Belo Horizonte (MG), Brazil
welbert@deelt.ufop.br, rass.eletrica@gmail.com,
aplc@ufmg.br

T. R. Oliveira, L. M. F. Morais, P. C. Cortizo,
Department of Electronic Engineering
Federal University of Minas Gerais (UFMG)
Belo Horizonte (MG), Brazil
troliveira@cpdee.ufmg.br, lenin@cpdee.ufmg.br,
porfirio@cpdee.ufmg.br

***Abstract*—This paper investigates a Solid State Transformer (SST) based DC microgrid architecture, addressing the design and control of the multiple SST power conversion stages and the power management strategy required for its integration with other microgrid elements, such as storage devices and local distributed generation. The advantages of a SST in relation to conventional low frequency transformers are commonly listed as a substantial reduction of volume and weight, fault isolation capability, voltage regulation, harmonic filtering, reactive power compensation and power factor correction. The SST also constitutes the required infrastructure that will enable DC power distribution to homes and commercial buildings in the near future and provides a more efficient way to integrate storage devices and distributed generation into the electrical grid. In this sense the SST behaves as an energy router, which represents a key element in an intelligent power system. The behavior of the proposed architecture for different operating conditions and disturbances will be assessed through computational simulations in the software MATLAB/*Simulink*.**

Keywords – Solid State Transformer; DC Microgrid; Smart Grid; Distributed Generation; Renewable Energy.

I. Introduction

Recently, the integration of distributed generation (DG) to the electric power system, as well as the diversification of loads connected to it, introduces the need for a distribution system with bidirectional power flow, local control and power management. This new system is referred as a "smart grid", whose concept involves the use of smart technologies, such as sensors, actuators and automation equipments, distributed throughout the electrical system and interconnected by a communication network. This new paradigm provides to the system players real time information concerning the electrical grid conditions, allowing the operation optimization and energy conservation. The application and real implementation of smart grids and in particular, *microgrids* – an extension of this concept for local power systems, are now being studied in various research centers [1], [2].

The microgrids provide several advantages, such as: *(i)* more efficient integration of distributed generators (wind, solar, biomass, etc.); *(ii)* transmission and distribution losses reduction, due to closeness between generation and consumption; *(iii)* presence of energy storage systems, which can supply the loads during demand peaks or temporary interruptions in generation; *(iv)* possibility to feed local loads in direct current, connecting them to a local DC bus; *(v)* greater interaction between the end consumer and the utility, when compared with the traditional electrical system and *(vi)* ease of differentiated and instantaneous measurements of power consumption in each consumer unit [3].

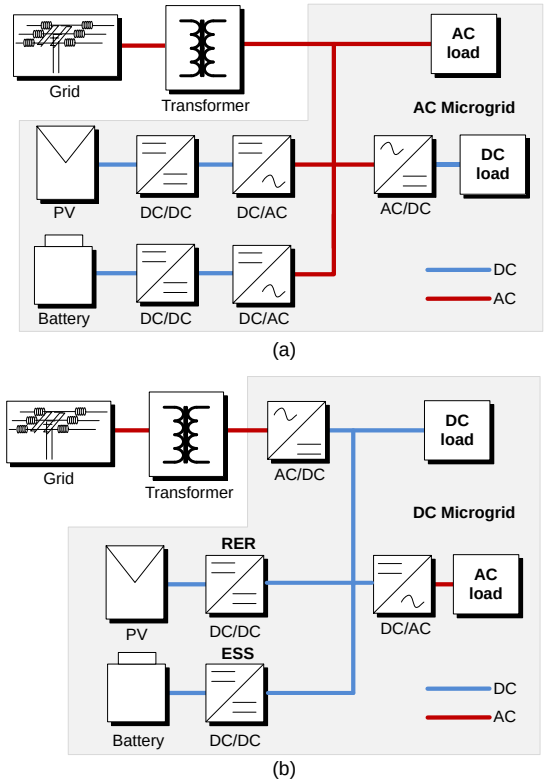

Fig. 1. Microgrid architectures: (a) AC microgrid, (b) DC microgrid.

Commonly, renewable energy generation and energy storage systems are key elements in DC and AC microgrids [4]. A traditional AC microgrid, illustrated in Fig. 1(a), can be connected to the distribution system in order to be a secondary power supply or to relieve the grid in peak demand periods. However, the various stages of DC-DC-AC conversion needed for connecting Renewable Energy Resources (RER) and Energy Storage Systems (ESS) to dc-links affect system efficiency. In a DC microgrid these unnecessary conversion

steps are eliminated and a AC-DC converter is adopted as the interface with the utility, as shown from Fig. 1(b). Therefore, there is a efficiency enhancement in DC microgrids [5].

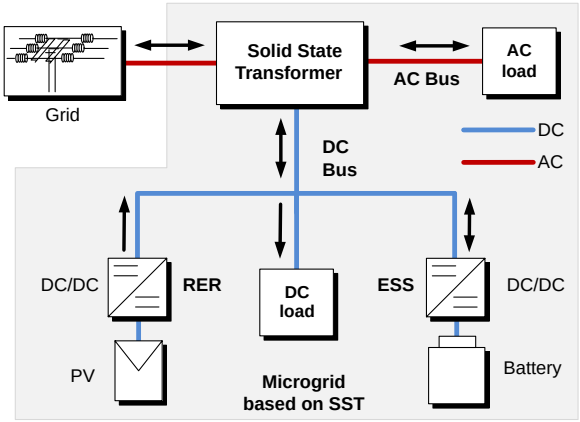

Fig. 2. Microgrid architecture based on SST.

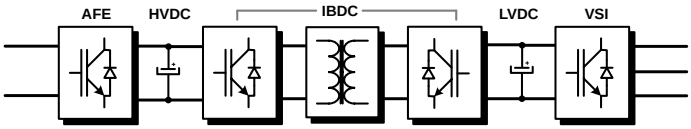

Fig. 3. SST topology based on three stages.

Typically, usual voltages in microgrids ($127\,V$ or $220\,V$ to AC loads and $380\,V$ for DC) are lower than medium voltage (MV) of distribution systems. Thus, AC and DC microgrids require an additional transformer for connection to MV distribution systems [16]. In this context, the conventional passive transformer does not meet the demands of microgrids. In fact, despite the wide use and robustness, the traditional transformer, designed for the frequency of $50/60\,Hz$, does not allow, for example: *(i)* control and voltage regulation (without the use of taps); *(ii)* local control of active and reactive power flow and *(iii)* the rejection of disturbances or anomalies from the MV primary circuit (harmonic distortion, short duration voltage variations, etc.) [5]. Furthermore, because of its low operating frequency, the conventional transformer is a heavy and bulky equipment.

Hence, in the context of microgrids, the Solid State Transformer (SST) is shown as an alternative to passive transformer. The SST basically comprises an AC-AC converter with input ("primary") at medium voltage and output ("secondary") at low voltage [5]. Fig. 2 shows the architecture of a SST based microgrid [6], in which the SST provides three interfaces with the system (primary, secondary and DC side). Roughly, a SST plays a role of three-port power router.

In this paper the architecture and control of a SST based microgrid are described, focusing on the discussion about the power stages that comprise the SST converter and the power management strategy that needs to be employed at its coupling point with a DC microgrid, in order to allow proper power flow and DC bus voltage stability. The behavior of the proposed system will be later verified through computational simulations, in order to evaluate the performance improvements in AC and DC distribution systems. The remainder of the paper is organized as follows: Section II describes the topology and control diagrams of the SST conversion stages. Section III discusses the DC microgrid power management strategy employed in the microgrid. Section IV presents the simulation results and Section V displays the paper conclusions.

II. Solid State Transformer Topology

For application in a microgrid system, the most suitable SST topology is that based on three stages, depicted in Fig. 3 [1]. In the first stage, there is a PWM rectifier (Active Front End, AFE), which is between the MV grid and the DC bus with highest voltage (denoted by HVDC in Fig. 3). The second stage includes an Isolated Bidirectional DC-DC Converter (IBDC), which performs power flow control between the HVDC bus and the Low Voltage DC bus (LVDC), to where the DC distribution is derived, and provides voltage level transformation and galvanic isolation. Accordingly, the IBDC plays the main role in the SST, since it adds the functions which are often desired to transformers. These functions are accomplished by a high frequency (HF) transformer, which also enables the volume reduction. The last stage is a Voltage Source Inverter (VSI), that feeds AC loads with a high quality sinusoidal and regulated voltage. The following subsections describe each SST stage, as well as the control techniques adopted in each one.

A. PWM Rectifier (AFE)

In a microgrid system, in which distributed generation and energy storage are incorporated in local power distribution, the front end rectifier must operate with bidirectional power flow and unity Power Factor (PF). Moreover, this stage must control the HVDC link and reduce the input current harmonic distortion at the point of common coupling to acceptable levels. As this stage deals with MV levels, which exceed the blocking capabilities of current power switches technology, a modular AFE topology adoption is advisable [3]. In order to meet those requirements, the modular SST topology presented in Fig. 4 is considered in this work. A three-phase LCL-filter interconnects the SST AFE stage to the utility, as shown in Fig. 4. Each converter phase comprises *n* "input-series and output-parallel" modules, each including a H-bridge rectifier and an IBDC.

The AFE control diagram is presented in Fig. 5(a) and deals with variables in a synchronous rotating frame ($dq0$). An external voltage control loop regulates the AFE modules HVDC busses to an average value V^*_{DC} through a PI compensator. This voltage loop not only provides HVDC regulation, but also enables the rejection of load transients. The output of the voltage loop produces the d-component reference for inductor current i. The q-component reference for inductor current is enforced to zero, in order to ensure the zero displacement between the grid current and grid voltage (e) and then, to attain $PF = 1$. An internal proportional current loop control is included for reference tracking and for rejecting disturbances introduced by transients in e. The PWM switching command for a converter phase is the same for all phase modules.

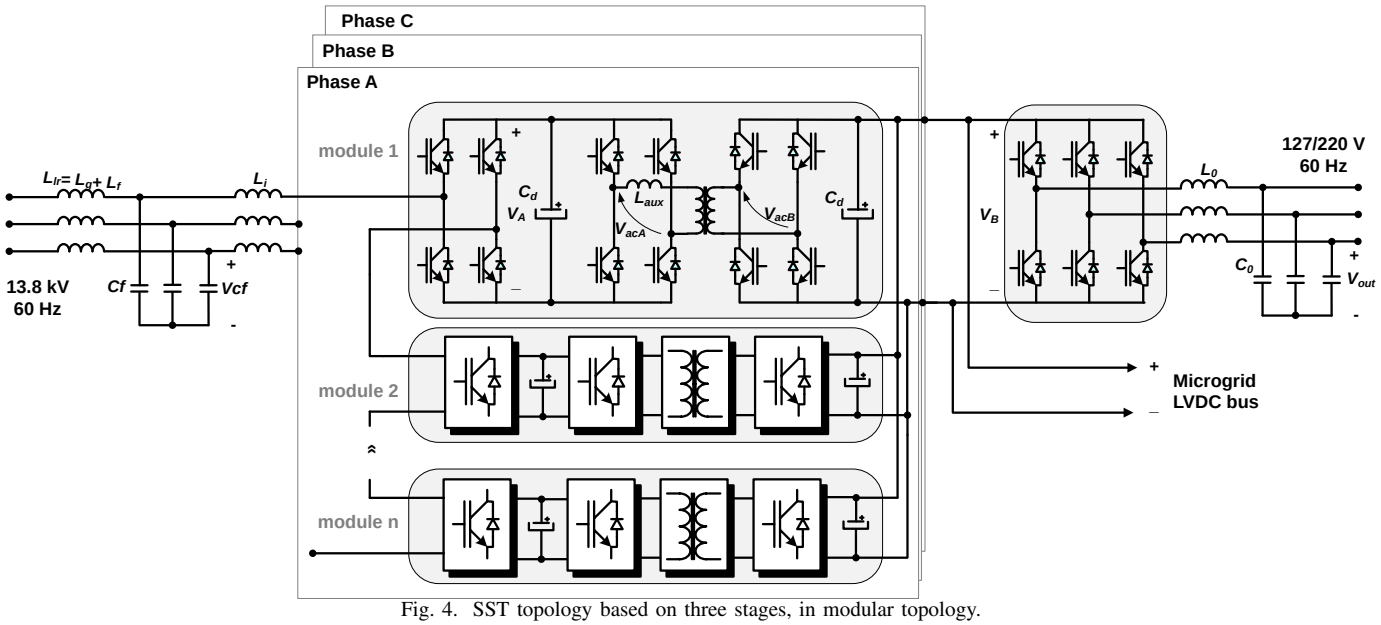

Fig. 4. SST topology based on three stages, in modular topology.

The concept of *dynamic stiffness* is used as a benchmark for evaluating control performance under disturbances, as proposed in [7]. Thus, the dynamic stiffness functions $|e/i|$ (1) and $|i_L/V_{HVDC}|$ (2) are derived, in which $V_{HVDC} = V_{DC}{\cdot}3n$ denotes the total HVDC bus voltage and V_{DC} is given in equation (3). While this first function indicates the magnitude of the grid voltage e required to produce a unit deviation in the inductor current i, the latter one measures the amplitude of the load current i_L needed to obtain a unit deviation in the HVDC bus voltage V_{HVDC}. The controller tuning problem is addressed by placing the zeros of those functions in the s-plane, in order to attain the desired robustness. The same approach for tuning control loops is discussed in [7] and will be omitted here.

$$\left|\frac{e}{i}\right| = sL_i + R_a \tag{1}$$

$$\left|\frac{i_L}{V_{HVDC}}\right| = s\frac{3C_d}{n} + k_p + \frac{k_i}{s} \tag{2}$$

$$V_{DC} = \frac{1}{3n}\sum_{i=1}^{3}\sum_{j=1}^{n} V_{ij} \tag{3}$$

B. Isolated Bidirectional DC-DC Converter (IBDC)

The IBDC converter must provide proper galvanic isolation and bidirectional power flow between the module HVDC bus and the LVDC common output. Although many possibilities could be considered for the IBDC implementation, perhaps the Dual Active Bridge (DAB) converter is the most adopted [8], and will be assumed here. This converter, shown in Fig. 4, consists of two H-bridges fed by the DC buses and connected by an HF transformer. The power flow control is mainly based on the angular displacement (ϕ) adjustment between the voltages denoted by V_{acA} and V_{acB} in Fig. 4. When the phase shift between these voltages is zero, there is no power flow between the converter bridges. For $\phi > 0$, the power flow is from A to B direction, and, for $\phi < 0$, the power flow is from B to A direction. The maximum power transfer is achieved when the phase shift (ϕ) is $\pm 90\,^{\circ}$. The transformer leakage inductance is the element responsible for the power flow between two bridges. However, depending on the desired amount of power transfer, it is needed to add an auxiliary inductor (L_{aux}) in series with the HF transformer [9].

Furthermore, the DAB converter provides the regulation of

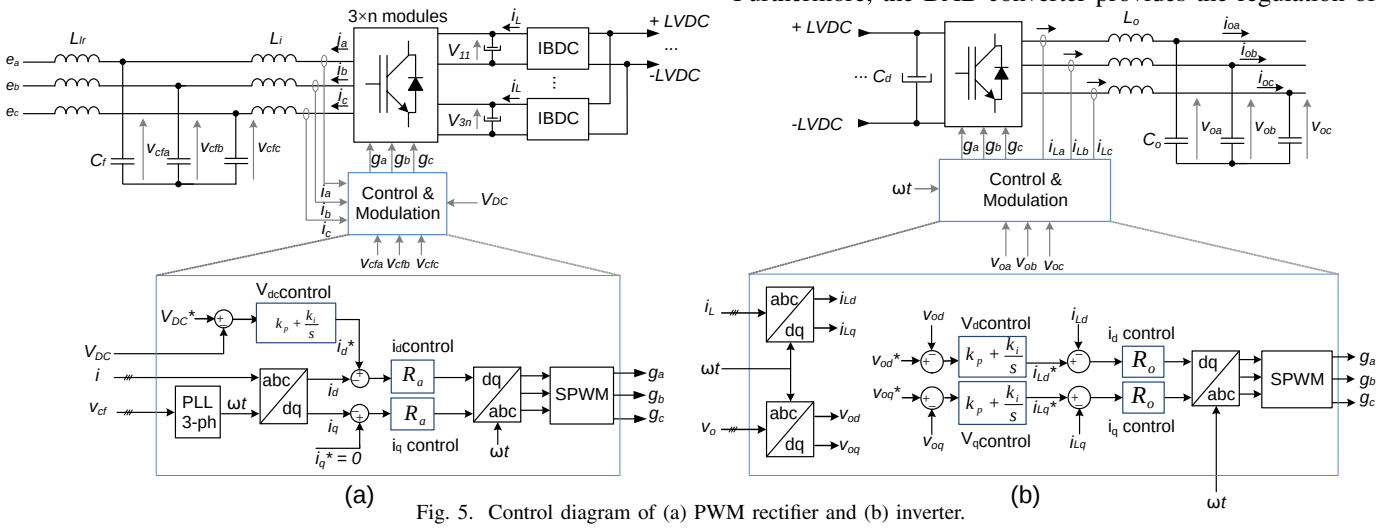

Fig. 5. Control diagram of (a) PWM rectifier and (b) inverter.

the output voltage, called V_B in Fig. 4, though the phase shift (ϕ) adjustment. The input voltage (V_A) is assumed constant in DAB design, since the rectifier control holds it approximately constant. The DAB output voltage control considers only a PI compensated voltage loop.

C. DC-AC converter (VSI)

The last stage of SST topology depicted in Fig. 4 is a three-phase voltage source converter (VSI). The control diagram of this converter is presented in Fig. 5(b) and includes an external loop for output voltage (v_o) control, followed by an internal loop, for controlling inductor current (i_L). Again, the controller gains are tuned by using the output voltage dynamic stiffness $|i_o/v_o|$ (4) as a benchmark for evaluating the control robustness to load current transients. The controllers are tuned as described in [7].

$$\left|\frac{i_o}{v_o}\right| = \frac{s^3 L_O C_O + s^2 C_O R_O + s k_p + k_i}{s^2 L_O} \tag{4}$$

III. DC MICROGRID POWER MANAGEMENT

A DC microgrid is constituted by the integration of Renewable Energy Resources (RER), an Energy Storage System and the SST LVDC bus. In order for those elements to operate in a coordinated fashion, ensuring proper power sharing and bus voltage stability, a power management strategy must be established. The use of a communication network and centralized control allows the execution of multiple tasks, such as voltage regulation and power flow optimization, however a communication failure can compromise the microgrid operation. Distributed methods, such as DC bus signaling (DBS) [10], [11], on the other hand confers higher reliability and a basic power flow management and can be incorporated in a hierarchical control structure, which can also provide optimal performance [2].

In this paper, the proposed power management method for the SST and DC microgrid integration is based on the DBS approach, in which a the LVDC bus voltage is allowed to vary inside a voltage window of $40\,V$ centered in the nominal value of $380\,V$. The voltage variation is used as a communication link to inform every converter of the microgrid load conditions and allow them to select a proper operation mode. The voltage window is divided in four $10\,V$ sectors in which each converter can operate as a voltage source (*voltage mode – VM*) or a current source (*current mode – CM*). In in VM the converter aids in LVDC bus voltage regulation. Fig. 6 depicts the static output behavior of the ESS converter and the SST modules LVDC output.

The RER converter is considered to operate in CM tracked to the PV array Maximum Power Point (MPP) in sector II-IV and in VM in sector I, so it limits the DC bus voltage rise due to power surplus. It can be noticed that the SST will be the main responsible for regulating the DC bus, in a way that it behaves as a constant $380\,V$ voltage source in a broad load range. If there is a power surplus, the ESS will tend to charge the batteries with a maximum charge current (I_{CMax}) and

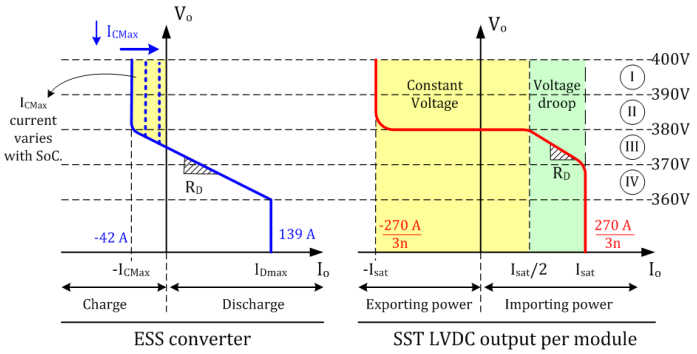

Fig. 6. DC Bus Signaling static behavior of the SST DAB output and ESS converter.

the SST will export power to the utility up to its maximum capacity (I_{Sat}). The maximum charge current is dependent on the charging method and the batteries State-of-Charge (SoC) and will vary during the microgrid operation. The ESS control system is described in [12] and will be omitted here. A power deficit will be dealt by the SST up to half its capacity. Beyond that the SST shifts to a droop behavior and the bus voltage will vary with the load increase. In sector III the ESS will reduce its consumed power, reaching a null condition in $375\,V$. Between $375\,V$ and $370\,V$ the ESS will inject power to the bus aiding the SST in voltage regulation. In sector IV, the SST has reached is full power capacity and the voltage regulation is solely related to the ESS. In VM, the droop characteristic observed in both converters static behavior is achieved with the insertion of a virtual resistance (R_D) in the voltage control loop reference, which is calculated to reach the converters maximum output power in the CM.

In any given situation, the DC bus signaling will allow the microgrid to adapt into a configuration that maintains the DC bus voltage inside the voltage window, while performing a basic power flow management. Therefore, voltage stability is guaranteed.

IV. SIMULATION RESULTS

A SST based DC microgrid computational model was built in the software MATLAB/*Simulink*, as depicted in Fig. 2, assuming an AFE rectifier with 6 series modules per phase and $100\,kVA$ rated power. In the LVDC bus, a $50\,kW$ PV-based RER and a $80\,kWh/50\,kW$ ESS, based on $12.6\,V/40\,Ah$ Li-ion devices, constitute the microgrid. The behavior of the proposed system is assessed by time simulation, assuming the parameters described in Table I and four operation scenarios: *(i) Case 1:* AC and DC load steps; *(ii) Case 2:* AC non-linear load step; *(iii) Case 3:* AC high voltage side voltage sag to $50\,\%$ in $t = 1.0\,s$; *(iv) Case 4:* AC low voltage single-phase ground fault, enforced in phase A at $t = 1.0\,s$. Table II presents the RER generation and load conditions in each scenario.

Fig. 7 exhibits the per unit voltage (black) and current (red) in phase A for the High Voltage (HV) and Low Voltage (LV) of the SST, the microgrid DC bus voltage and currents injected by the SST second stage (red), RER converter (black) and

TABLE I
SIMULATION CONDITIONS.

Parameter	Value
Rated AC frequency	$60\,Hz$
1-ϕ Base power	$33.3\,kVA$
1-ϕ RMS Bases in SST HV side	$7.97\,kV$/ $4.18\,A$
1-ϕ RMS Bases in SST LV side	$127\,V$/ $262.43\,A$
SST AC line voltages (RMS)	$13.8\,kV$/ $220\,V$
HVDC bus voltage for each module	$3.166\,kV$
LVDC bus voltage	$380\,V$
Switching frequency	$10\,kHz$
AFE input filter [L_{lr}, L_i, C_f]	[$0.5H$, $636mH$, $23.2nF$]
VSI output filter [L_O, C_O]	[$256\mu H$, $100\mu F$]
DC bus capacitor (C_d)	$2.2\,mF$
DAB auxiliary inductance (L_{aux})	$25\,mH$
AFE compensators gain [R_a, k_p, k_i]	[24kΩ, $2.765S$, $694.8S/s$]
VSI compensators gain [R_O, k_p, k_i]	[23Ω, $5.7S$, $2.87kS/s$]
Voltage mode droop (R_D) [DAB, ESS]	[0.999 Ω, 108 $m\Omega$]
RER maximum capacity	$50\,kW$
ESS rated storage capacity and power	$80\,kWh$ / $50\,kW$
ESS maximum charge/discharge current	$42\,A$ / $139\,A$

ESS (blue). As it can be noticed, at $t = 0.5\,s$ an AC load step occurs, leading to a LVDC bus temporary decrease to $87\,\%$. The RER output current is not significantly affected, but the SST reacts to the voltage change and raises its injected current from $10.6\,A$ ($4\,kW$) to $103\,A$ ($39\,kW$). The ESS, which initially consumed $28\,A$ ($10.7\,kW$), perceives the voltage swing and reduces its consumed power during the bus transient. As the DC bus voltage converges to $380\,V$, the charge current tends to increase up to $42\,A$. At $t = 1.1\,s$, the DC load step also leads to a DC bus transient. The increase in consumed power forces the SST to enter droop mode, which reduces the steady state voltage level to $372\,V$. The SST ends up injecting $189\,A$ ($70\,kW$) and the ESS supplies $26\,A$ ($9.7\,kW$) to aid in voltage regulation. The system is also able to decouple the input and output dynamics, since the HV side current shows a smooth variation even with abrupt load steps. It can be seen as well that the SST compensates the AC $220\,V$ bar 0.9 power factor, attaining unity power factor at the HV side.

Fig. 8 displays the system behavior to the connection of a $36\,kW$ non-linear load to the AC $220\,V$ bar at $t = 1.0\,s$. Initially the ESS converter charges the battery bank with maximum charge current ($42\,A$) and the SST supplies $26\,A$ to regulate the DC bus to $380\,V$. After the load step, the inrush current of the three-phase rectifier forces the bus voltage to sink, which affects the VSI output voltage and current. In steady state, the system enters droop mode, with $374\,V$ ate the DC bus. The ESS consumes $18\,A$ ($6.7\,kW$) and the SST provides $34.8\,kW$ and the harmonics required by the VSI. The high harmonic content in the VSI output current distorts its output voltage around the sinus peak, however, such disturbance is not propagated to the HV side, or to the DC bus,

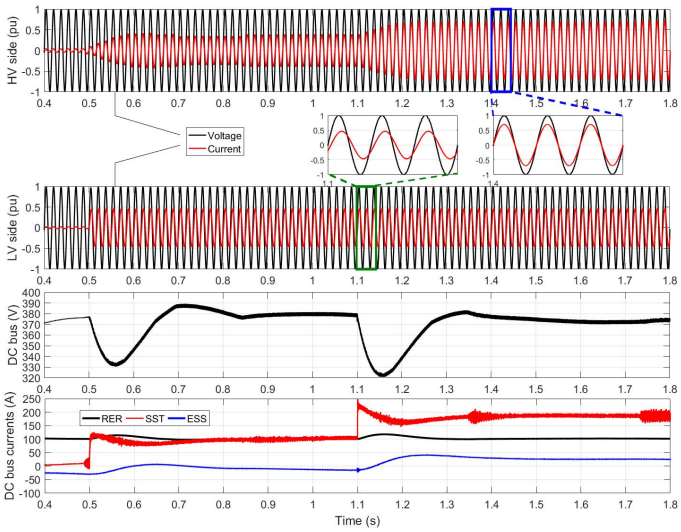

Fig. 7. Simulation results under load current step variation.

i.e., a high power quality is still ensured to the utility grid and the DC microgrid.

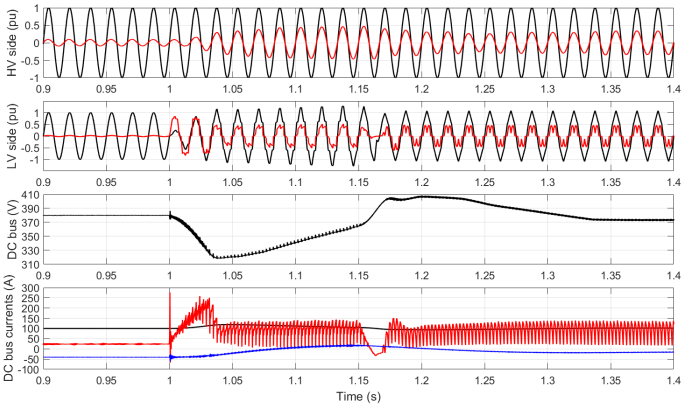

Fig. 8. Simulation results when supplying a non-linear load.

Fig. 9 presents the system response to a voltage sag to $50\,\%$ at the HV side. It can be observed that during the sag the SST input current is saturated by the AFE, but no influence is noticed at the DC bus and AC low voltage side. It shows that the SST can provide ride through capabilities to the DC microgrid and decouple the LV side from disturbances in the medium voltage distribution system.

Fig. 10 shows the system behavior against a single-phase ground fault at the AC low voltage side. It can be noticed that the VSI is able to limit the fault current in $1\,p.u.$, which prevents damages to the SST and distribution system. A slight transient is observed in the DC bus and the consumed power is also increased. The ESS aids with voltage regulation but the SST is responsible for supplying the negative sequence current required by the VSI. Once again, such disturbance at the LV side is not propagated to the HV side.

V. CONCLUSION

This paper presented the structure of a modular three-stage SST based DC microgrid with DC bus signaling primary

TABLE II
SCENARIOS STUDIED IN SIMULATIONS.

Parameter	Case 1	Case 2	Case 3	Case 4
AC load (220 V bar)	$2.4\,kW$ $(0 < t \leq 0.5\,s)$ $42.4\,kW/20\,kVar$ $(t > 0.5\,s)$	$2.4\,kW$ $(0 < t \leq 1.0\,s)$ *$38.7\,kW$ $(t > 1.0\,s)$	$42.4\,kW/20\,kVar$	$42.4\,kW/20\,kVar$
DC load	$28.9\,kW$ $(0 < t \leq 1.1\,s)$, $74\,kW$ $(t > 1.1\,s)$	$28.9\,kW$	$28.9\,kW$	$28.9\,kW$
PV generation	$38\,kW$	$38\,kW$	$38\,kW$	$38\,kW$

*A $36\,kW$ 3ϕ diode rectifier with filter is connected to the AC $220\,V$ bar, representing the non-linear load.

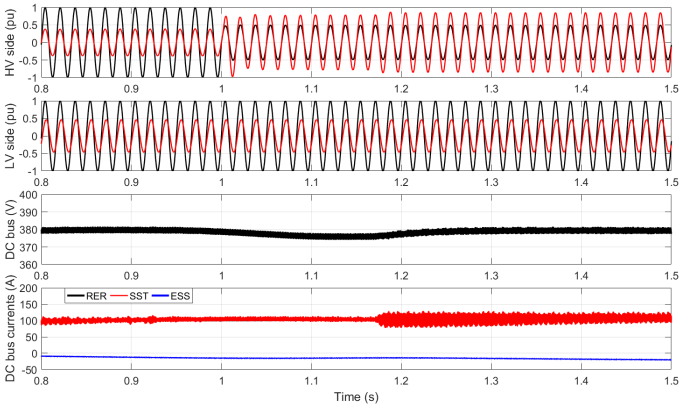

Fig. 9. Simulation results during a voltage sag.

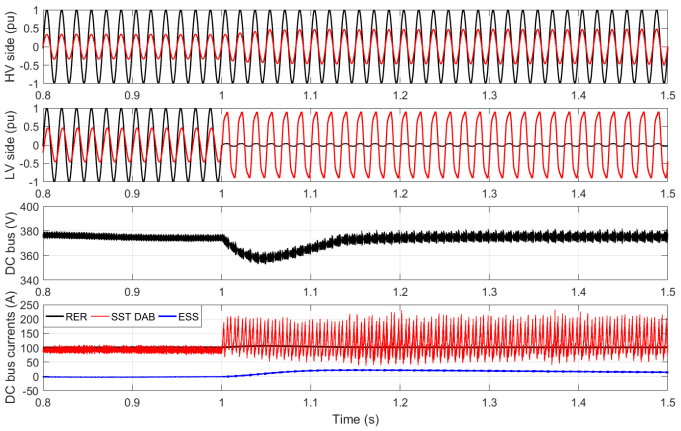

Fig. 10. Simulation results in a single-phase fault condition.

control and verified its behavior against distinct operation conditions. It is a consensus that the SST can provide significant weight and volume reduction, in comparison with conventional distribution transformers, along with smart features. The simulations carried out in this paper shows that a SST based microgrid, besides those advantages can also provide: *(i)* compensation of utility grid disturbances, e.g., voltage sags; *(ii)* fault protection, due to the converters current limiting capabilities; *(iii)* power factor correction; *(iv)* AC input-output decoupling and isolation, hence disturbances occurred in one side of the SST do not propagate to the other side; *(v)* possibility to accommodate DC power distribution, and *(vi)* ease of renewable energy resources and energy storage integration with the AC utility and low voltage distribution grid, due to DC bus power management and SST bidirectional power flow.

Furthermore, the SST could replace several equipments of electrical systems which are added specifically to perform the aforementioned functions, namely capacitor and reactor banks, active filters, synchronous compensators, STATic synchronous COMpensators (STATCOMs), Static Var Compensators (SVCs), Dynamic Voltage Regulators (DVRs) and Unified Power Flow Controllers (UPFCs), leading to a simpler and more efficient power system, towards the deployment of a smart grid.

ACKNOWLEDGMENT

The authors would like to thank FAPEMIG for the financial support conferred to this project.

REFERENCES

[1] S. Roy, A. De, and S. Bhattacharya, "Multi-port Solid State Transformer for Inter-grid Power Flow Control," in *2014 International Power Electron. Conference, Hiroshima – ECCE*, vol. 1, 2014, pp. 3286–3291.

[2] J. M. Guerrero, J. C. Vásquez, and R. Teodorescu, "Hierarchical control of droop-controlled DC and AC microgrids – A general approach towards standardization," *IECON Proceedings (Industrial Electron. Conference)*, pp. 4305–4310, 2009.

[3] R. H. Lasseter, "Smart Distribution: Coupled Microgrids," *Proceedings of the IEEE*, vol. 99, no. 6, pp. 1074–1082, 2011.

[4] X. She, S. Lukic, A. Q. Huang, S. Bhattacharya, and M. Baran, "Performance evaluation of solid state transformer based microgrid in FREEDM systems," in *Conference Proceedings – IEEE Applied Power Electron. Conference and Exposition – APEC*, 2011, pp. 182–188.

[5] B. Zhao, Q. Song, and W. Liu, "Power characterization of isolated bidirectional dual-active-bridge dc-dc converter with dual-phase-shift control," *IEEE Trans. Power Electron.*, vol. 27, no. 9, pp. 4172–4176, 2012.

[6] J. W. V. D. Merwe and H. du Mouton, "The Solid-State Transformer Concept: A New Era in Power Distribution," in *AFRICON 2009*, 2009.

[7] M. Ryan and R. Lorenz, "A high performance sine wave inverter controller with capacitor current feedback and and BACK-EMF decoupling," in *Proceedings of Power Electron. Specialist Conference*, vol. 1, 1995.

[8] F. Krismer, "Modeling and Optimization of Bidirectional Dual Active Bridge DC DC Converter Topologies," Ph.D. dissertation, Techische Universität Wien, 2010.

[9] H. Zhu, Y. Li, P. Wang, Z. Li, and Z. Chu, "Design of Power Electronic Transformer Based on Modular Multilevel Converter," in *2012 Asia-Pacific Power and Energy Engineering Conference*, 2012, pp. 1–4.

[10] J. Schoenberger, R. Duke, and S. D. Round, "Dc-bus signaling: A distributed control strategy for hybrid renewable nanogrid," *IEEE Trans. on Industrial Electron.*, vol. 53, no. 5, pp. 1453–1460, 2006.

[11] D. Boroyevich, I. Cvetkovic, D. Dong, R. Burgos, F. Wang, and F. Lee, "Future electronic power distribution systems – a contemplative view," in *12th International Conference on Optimization of Electrical and Electronic Equipment (OPTIM)*, May 2010, pp. 1369–1380.

[12] T. R. Oliveira, W. W. A. G. Silva, and P. F. Donoso-Garcia, "Distributed secondary level control for energy storage management in dc microgrids," *IEEE Trans. on Smart Grid*, vol. PP, no. 99, pp. 1–11, 2016.